OPEN ACCESS
IOP Publishing
Journal of Optics
J. Opt. **17** (2015) 125615 (8pp)
doi:10.1088/2040-8978/17/12/125615

Demonstration of spot size reduction by focussing amplitude modulated radially polarized light on a photoresist

K Ushakova, Q Y van den Berg, S F Pereira and H P Urbach

Optics Research Group, Department of Imaging Physics, Faculty of Applied Sciences, Van der Waalsweg 8, Delft 2628CH, The Netherlands

E-mail: k.ushakova@tudelft.nl and s.f.pereira@tudelft.nl

Received 11 June 2015, revised 18 August 2015
Accepted for publication 20 August 2015
Published 11 November 2015

Abstract

Spot size reduction is demonstrated by printing focused spots from amplitude-modulated radially polarized light at the wavelength $\lambda = 405$ nm on a photoresist. Amplitude modulation is realized by ring illumination and by application of an optimized amplitude distribution function. Amplitude modulation is implemented via spatial light modulator, which is followed by a specially designed radial wire grid polarizer to obtain high-quality radially polarized light. Comparison between full and amplitude modulated apertures of the written focused spots on a photoresist is performed. Rigorous simulations based on the Richards-Wolf integral are made to confirm experimental data.

Keywords: lithography, focussed radially polarized light, amplitude modulation, near UV light

1. Introduction

An increasing interest in the minimization of the focused spot size while maintaining the circular symmetry in high numerical aperture optical systems has been observed in the last few decades [1–4]. In the pioneering work of S. Quabis *et al*, it has been shown that if one uses radial polarization, a very sharp spot is obtained for the longitudinal component of the focused light field [5]. This sharp focused longitudinal component has been used in several applications such as optical trapping [6, 7], plasmonics [8], laser machining [9, 10], accelerators [11], and single molecule detection [12]. One problem that limits the application of focused radially polarized light is the fact that although the longitudinal component is the strongest component of the field (in the case of very high numerical aperture) and has a spot-like distribution, there also exists a transversal component in focus with a doughnut-like distribution. As a consequence, in applications where the total intensity distribution of the field is relevant, the resulting spot of radially polarized light is cylindrically symmetric and narrower than the Airy spot [5]. Also, if there is an interface between the lens and the focused field region from a low to high index of refraction, as is the case with the commonly found air/medium interfaces in many focussing applications, the ratio of energy distribution between the longitudinal/transversal component gets worse, since the geometrical numerical aperture inside the medium is smaller than in the air [13]. One way to modify the relative intensity distribution of the longitudinal and transversal components in focus is to apply amplitude and phase modulation in the pupil of the focusing lens. In [14–18], the authors successfully showed that considerable reduction of the transverse component can be achieved using beam shaping. Our motivation to the present research is to print spots in focus on a photoresist that can be 20–30% smaller in size than the conventional spots that are obtained with linear polarization. This opens directly a large field of possible applications such as confocal microscopy [19, 20], maskless lithography, direct laser writing [21–23], and optical tweezers [24–26].

Experimental realization, followed from the theoretical predictions, shows that obtaining high-quality radially polarized beams, before focusing, plays a crucial role in getting

minimized focused spot. This inspired the development of a variety of methods of radially or azimuthally polarized light formation, e.g., such as interferometrically [27], by spatial light modulator (SLM) [28, 29], liquid crystal devices [30, 31], optical fibers [32, 33], spatially variant sub-wavelength grating [34], and wire-grid polarizers with cylindrical symmetry [35]. In this work, we have chosen to use the latter method since good quality radially polarized beams can be achieved, and it can be extended to the UV spectral range, which is relevant in photoresist applications. One can obtain good extinction of the azimuthal polarization (1/2000) with the wire-grid polarizer, and there are no defects/diffraction effects. Our wavelength is 405nm, which is the edge wavelength of the liquid crystal devices, such as the device mentioned in [36]. Further, for future applications with resists, lower wavelengths should be used, and liquid crystals are no longer an option.

In the first section of the paper, we briefly present the basic theory that has been studied in [37] and show the optimized pupil distribution to achieve the sharpest focused field of the longitudinal component while minimizing the contribution of the transversal component when the light is focused through an interface. The second section describes experimental methods, set-up, and instrumentation used to implement amplitude and polarization shaping to the beam and to use it to focus the light with high numerical aperture objective on a photoresist. In 'Results and Discussion', comparative analysis of the experimental and theoretical data is performed as well as evaluation of the different ways to obtain minimized focused spot. Finally, we conclude the paper by highlighting important points.

2. Theory

Radially polarized beams are a special case of cylindrical vector beams that are symmetric in their polarization around the axis of propagation [38]. In cylindrical coordinates (r, ϕ, z), the vectorial electric field $\mathbf{E}(\mathbf{r})$ of a propagating, monochromatic beam with wavenumber $k = 2\pi/\lambda$ can be written as

$$\mathbf{E}(\mathbf{r}) = A(r)\,\hat{\mathbf{e}}_r, \tag{1}$$

where $\hat{\mathbf{e}}_r$ is a unit vector and $A(r)$ represents an arbitrary amplitude function, which vanishes for $r = 0$. In this work we can approximate the amplitude of our beam with a top-hat function. When such a beam is tightly focused using a high-NA objective, the off-axis rays are in particular strongly bent. When focusing in air, this results in an electric field in the focal region in which the longitudinal component is dominant [5, 13, 39]. Interestingly, the longitudinal electric field in the focal plane is much more confined than the transverse electric field [40].

In this paper we use optical lithography to print spots by means of monochromatic light with a wavelength of 405 nm with a high numerical aperture 0.9 NA objective for use as an experimental reference. In this context, radially polarized beams are tightly focused through an air-photoresist interface.

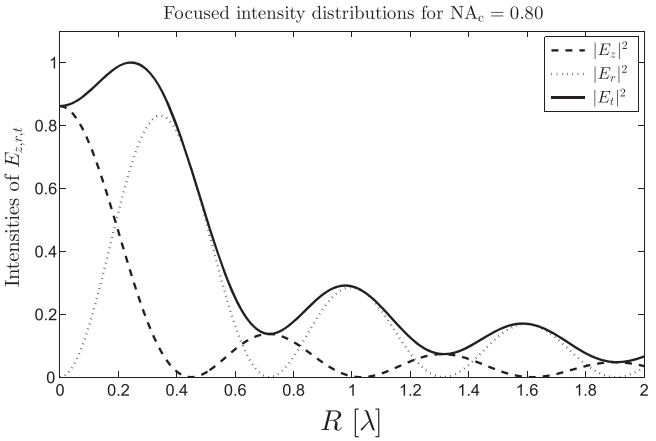

Figure 1. Vectorial electric field in focal plane inside photoresist in a.u [42]. E_z denotes the longitudinal field, E_r the transverse field, and E_t the total field and R the distance from the optical axis in wavelength units.

This has a significant impact on the vectorial electric field in focus through the angle-dependent transmission and reflection coefficients each ray encounters.

Thus, in order to make a better prediction of the spot size inside the resist, we should take these effects into account. The Shipley 1805 photoresist with a 300 nm layer thickness and a refractive index $n_{\text{res}} = 1.68 + i \cdot 0.020$ for the 405 nm wavelength is used. We assume the focal plane is placed at a depth of 130 nm inside the photoresist. Due to the interface, the longitudinal field inside the photoresist is weakened. In order to compensate, we will modulate the incoming beam to increase the off-axis intensity in the object plane. The most basic form of amplitude modulation to achieve this is to block the beam center with a binary amplitude mask that transmits only rays with a deflection angle larger than

$$\alpha_{\min} \equiv \arcsin\left(\text{NA}_c/n\right), \tag{2}$$

where NA_c defines a cut-off numerical aperture. By using a threshold of $\text{NA}_c = 0.8$, the longitudinal field in focus becomes as large as the tranversal field as observed in figure 1 as computed with the Richards and Wolf diffraction integral [41, 42]. The squared modulus is plotted for each component as this is proportional to their intensity contribution. Experimentally, the total intensity distribution will be recorded, but increasing the relative contribution of the longitudinal field makes the total spot size smaller.

It is also interesting to observe how the spot size changes with aperture blocking for radial polarization, as well as linear polarization. The spot size in figure 2 is defined as the full width at half maximum (FWHM) of the total intensity. For apodization beyond $\text{NA}_c = 0.70$, the FWHM spot size with radial polarization becomes smaller than that of linear polarization. This is the regime we will focus on with our experiments.

Lastly, we can expect that the focal depth of the focused field inside the photoresist will be longer than for the case of focusing in air since the convergence angle of all rays, as seen

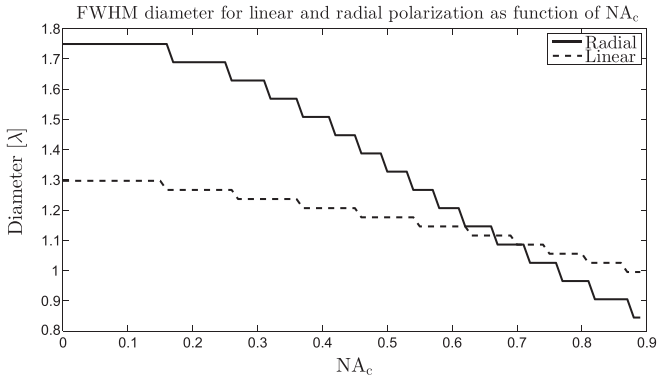

Figure 2. FWHM diameter of the total intensity distribution in the focal plane inside photoresist for linear and radial polarization.

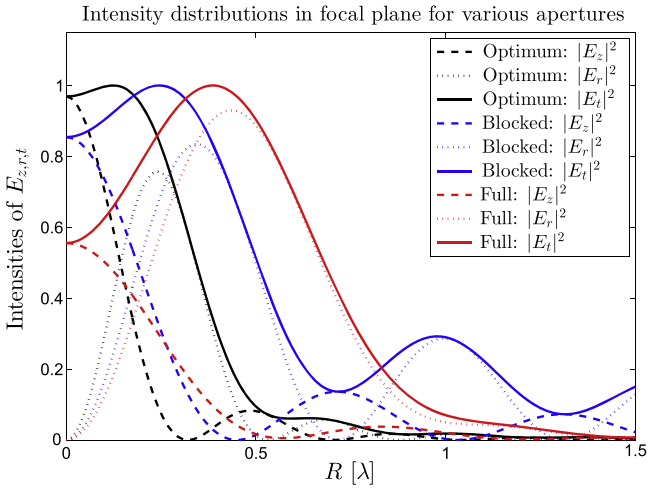

Figure 3. Normalized intensities of the electric fields in focus for the optimum aperture (black), full aperture (red), and blocked aperture with $NA_c = 0.70$ (blue). E_z denotes the longitudinal field, E_r the transversal field, and E_t is the total field. The focal plane is located 130 nm into the photoresist.

from the focal point inside the medium, is reduced in comparison with the case of focusing in the air.

A binary amplitude mask turns out not to be the optimum pupil function to generate the largest longitudinal field in focus, although it still reduces the FWHM of the Airy disk in focus. Along the same lines as [37], the optimum pupil function was derived by writing the electric field in focus as an arbitrary plane-wave expansion and maximizing the longitudinal field component under a constant power constraint. As the light is focused through an interface, each plane wave of the electric field expansion undergoes an additional refraction taken into account through its angle-dependent Fresnel transmission coefficient. The power constraint was imposed by means of a Lagrange multiplier, resulting in an analytic expression for the plane-wave expansion that maximizes the longitudinal field in focus. The optimum pupil field $A(\theta)$ can be derived from the plane-wave amplitudes by using the vector diffraction theory for a lens in [43] where the mathematical details on this calculation can also be found. Through the transformation of the radial pupil coordinate $r = f \sin\theta$, where f denotes the focal length of the lens and θ the refraction angle, the optimum pupil field, obtained when the absorption in the second medium is neglected, is represented here in its angle-dependent form:

$$\mathbf{A}(\theta) = \frac{1}{\Lambda}\frac{\sqrt{\cos\theta}}{\lambda f n_{\mathrm{res}}} \cdot \sqrt{\frac{\mu_0}{\epsilon_0}}\tan(\theta) \times t_p\big(\theta;\, n_1 = 1,\, n_2 = \mathrm{Re}\{n_{\mathrm{res}}\}\big)\,\hat{\mathbf{e}}_r, \tag{3}$$

where n_{res} is the photoresist refractive index and t_p denotes the Fresnel transmission coefficients for p-polarization. In our research, $n_1 = 1$ is chosen to represent an air/resist interface. The scalar parameter Λ can be tuned to modify the total power flow passing through the lens:

$$\Lambda = \frac{\sqrt{\pi}}{\sqrt{\mathrm{P}_0}}\frac{n_1^{3/2}}{\lambda n_{\mathrm{res}}}\left(\frac{\mu_0}{\varepsilon_0}\right)^{1/4} \cdot \left(\int_0^{\theta_{max}} \left|t_p(\theta)\right|^2 \sin^3\theta \mathrm{d}\theta\right)^{1/2} = 0.3272\frac{\sqrt{\pi}}{\sqrt{\mathrm{P}_0}}\frac{n_1^{3/2}}{\lambda n_{\mathrm{res}}}\left(\frac{\mu_0}{\varepsilon_0}\right)^{1/4}, \tag{4}$$

where P_0 is the power flow through a transversal plane and the integral in equation (4) is numerically evaluated for the case NA = 0.9. The optimized pupil field is also radially polarized, but its amplitude is a continuous, monotonously increasing function with distance from the optical axis. In later sections, (3) will be referred to as the optimum aperture function.

Figure 3 summarizes our motivation for shaping the aperture amplitude. A uniform intensity distribution in the lens pupil leads to an intensity distribution in the focal plane with a FWHM diameter of 1.40λ. By blocking the beam center with a threshold $NA_c = 0.70$, the FWHM diameter reduces to 1.02λ. The optimum aperture function has a FWHM total intensity of 0.72λ, almost a factor 2 reduction as compared to the unmodulated beam.

3. Experiment

3.1. Resist samples preparation, exposures, and development

For the experiments, we use resist with a positive tone, Shipley 1805 deposited on glass. In our case, it is desirable to create a resist layer with a thickness of less than 300 nm to assure the focused spot is within the depth-of-focus of the optical system and avoid standing wave effects (since the reflection between resist and glass can be neglected). For this purpose, the resist was diluted with its original solvent, Propylene Glycol Monomethyl Ether Acetate (PGMEA), in a 1:1 ratio and the layer was deposited with a spinning velocity of 2000 rpm. The photoresist thickness was verified using a profiler. In order to stabilize the layer and ensure a good development process, the resist was prebaked (before exposure) at an optimized temperature of 110 °C for 2 min. The development of the sample is done in solution of Microposit Concentrate: demineralized water = 1:2 for 30 s and stopping in demineralized water for 30 s.

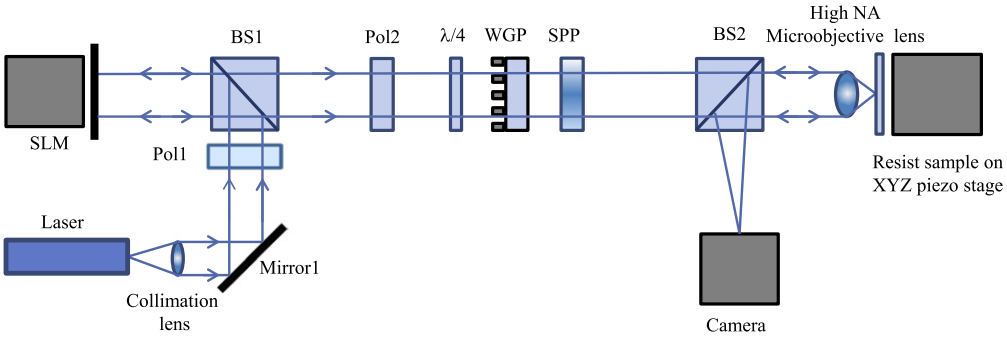

Figure 4. Scheme of the set-up to print focused radially polarized light spots arrays: Laser—405 nm diode laser; Collimation lensbuilt-in lens made especially for $\lambda = 405$ nm; Mirror1 mirror for $\lambda = 405$ nm; Pol1-Pol2 Glan Laser polarizers; BS1, BS2 beam splitters; $\lambda/4$ quarter wave plate; WGP wire-grid polarizer; SPP spiral phase plate for $\lambda = 407$ nm; Camera; High NA Objective lens with NA = 0.9.

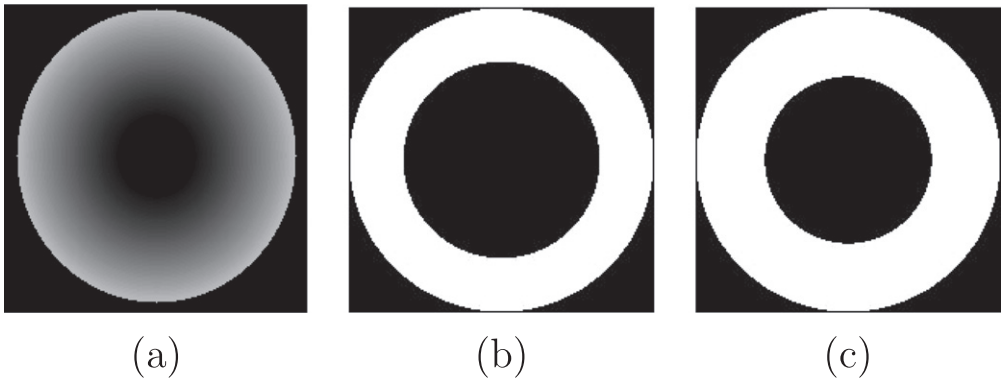

Figure 5. Pixelated for the SLM optimum amplitude function: (a) reduced aperture $0.80 < \mathrm{NA} < 0.90$ (b), and $0.75 < \mathrm{NA} < 0.90$ (c) modulated function. White and black colors are associated with the maximum and minimum amplitude of light (in reflection) correspondingly.

3.2. Set-up

The set-up to demonstrate the effect of the amplitude modulation of the focused radially polarized light is presented in figure 4. The diode laser of wavelength of 405 nm has a flat-top intensity distribution with a diameter of d = 3.8 mm and can be shaped in amplitude by the combination of two polarizers Pol1 and Pol2 and the spatial light modulator (Holoeye LC-R2500). After Pol2, the beam passes through a quarter lambda plate, a wire-grid polarizer (WGP), and a vortex phase plate (RPC photonics) to convert the beam from linear to radial polarization with all polarization vectors in phase [38, 44]. The WGP, consisting of concentric hollow aluminium cylinders of height h = 100 nm, period p = 200 nm and width of aluminium walls of w = 150 nm (i.e., filling factor f = 3/4) on a glass substrate was specially designed and fabricated to form near a UV-VIS high-quality radially polarized light convertor, in particular, at the wavelength of 405 nm with an extinction ratio of radial and azimuthal components R(405 nm) = 2000. The smallest and largest hollow cylinders have outer radii of 400 nm and 2 mm (radius of the WGP), correspondingly. Fabrication was performed based on electron beam exposure and development of the e-beam photoresist ZEP520A covering sputtered aluminium layer and subsequent chlorine-etching technique followed by removal of the residuals of the resist by oxygen plasma cleaning. Since the WGP has a cylindrically symmetric geometry, the radial electric field component (associated with the transverse magnetic (TM) polarization component, of which the electric field is perpendicular to the grooves) is transmitted, whereas the transmission of the transverse electric (TE) polarization component (parallel to the grooves) is suppressed, when the grating period is smaller than $\lambda/2$. The radially polarized beam is focused by an objective with a numerical aperture NA = 0.9 on the glass sample with the photoresist. The sample is mounted on a NanoCube XYZ closed loop piezo-driven stage.

As was discussed in section 2 the marginal rays of a radially polarized beam make the largest contribution to the longitudinal field E_z in focus. Adjusting the aperture transmission so that it selects only these rays allows us to strengthen the longitudinal field in focus. With the spatial light modulator (SLM) adjusted for amplitude modulation, it is possible to introduce a customized amplitude aperture function. Exposures with the presence of full aperture (unmodulated radially polarized beam), reduced apertures obtained by blocking the beam center up to NA = 0.75, 0.8 and optimum amplitude function (according to section 2) given by equation (3) were made (see figure 5). The SLM is an amplitude-only device that operates in reflection mode, and no pixel-dependent additional phase change is induced by it. In the experiment, we use an automatic procedure of 2D

Table 1. Parameters of the exposure experiment. (∗ - optimum pupil field distribution according to the optimum plane wave amplitudes given by equation (3) of section 2).

	$0 < \mathrm{NA} < 0.9$	$0.75 < \mathrm{NA} < 0.9$	$0.8 < \mathrm{NA} < 0.9$	$\mathbf{E}^p(\theta)^*$
Power, μW	6.76	6.3	5.51	2.17
Initial exp. time, ms	1	40	75	45
Dose, nJ	6.76	252	413	97.65

array writing, which is implemented by means of a Lab View program that simultaneously controls the laser via pulse generator (Tabor 8600) and the piezo stage position. Each spot in the printed 2D array is associated with certain exposure time (by adjusting the length of the laser pulse) and through focus position, which are varied from spot to spot by the XYZ piezo. Increases of exposure time with a step of $\Delta t = 1$ ms and through focus $\Delta z = 100$ nm were performed. The through focus position is varied by moving the piezo in z-direction. The XYZ piezo was tested for linearity before use. After every movement of the piezo, there was a waiting time of 2 s applied to ensure a complete stabilization of the piezo before the actual exposure with a laser pulse. Recorded arrays are the evidence of the piezo stability in the XYZ directions, since there are no shifts/printing failure of rows/columns and there are clear through-focus movements.

The parameters of exposures are summarized in table 1. Printed spots of equal depth are further compared. The dose varies for different cases of the amplitude modulation, since there is a different spatial distribution of energy for each of them.

3.3. Inspection of the samples

After development of the samples with exposed resist the best focus spot arrays are inspected first with an optical microscope, as shown in figure 6, to quickly select the samples with arrays that are printed at a certain depth by the combination of the exposure time above, threshold, and through-focus positions. The size of the best focus spots can not be analyzed with an optical microscope because of the resolution limit. Therefore, to analyze them, an AFM (atomic force microscope) was also used. The depth of the removed resist within the spots of array (parameter under interest) can also be extracted with the AFM. The topography data scans of the written arrays were made using a Bruker AFM. A fast scan head was used to speed up data acquisition with a maximum scan size of 36×36 μm^2. The choice of the best focus spots is made according to the largest depth parameter values via comparison of the depth values for each column of the equal focus position spots. The depth of the spots in the best focus spots varies for arrays of different intensity amplitude modulation. This is due to the redistribution of energy within the beam cross-section, linear resist reaction response for intensities in the region before saturation (complete over-exposure of the resist when the spot reaches the substrate), and nonlinear jump edge for the border of the resist reaction to the exposure dose. In figure 7 the best focused spots are framed for the four cases of amplitude modulation.

Figure 6. Optical microscope image of the example of an array printed with unmodulated beam intensity profile.

4. Results and discussion

Figure 8 presents the raw profiles of a printed spot obtained from the AFM data for the various amplitude modulation schemes: no amplitude modulation, central blocking with $\mathrm{NA} < 0.75$, central blocking with $\mathrm{NA} < 0.8$, and optimum aperture function. FFT (fast Fourier transformation) and Gaussian fitting are applied to extract parameters of FWHM, depth, and contrast. After analysis of the data extracted from figure 8 for the various cases of amplitude distribution in the pupil, the comparison of these different cases of beam modulation is made. In figure 8, the profiles of the spots with approximately the same depth for the unmodulated intensity beam profile ($0 < \mathrm{NA} < 0.90$), modulated intensity beam profile of reduced apertures ($0.75 < \mathrm{NA} < 0.90$, $0.80 < \mathrm{NA} < 0.90$), and optimum aperture function are represented by black, yellow, red, and magenta curves, respectively. Full aperture and reduced aperture of $0.80 < \mathrm{NA} < 0.90$ best focus spots of the higher depth were printed and therefore can be compared directly. The FWHM of the best focused spot corresponding to the reduced aperture of $0.80 < \mathrm{NA} < 0.90$ is 47% smaller than the one full NA $0 < \mathrm{NA} < 0.90$ for depths of spots of d $\sim$140 nm (see figure 8(b)). At a smaller depth, it was possible to compare spots obtained with all amplitude modulation functions (see figure 8(a)). In this case the spot size with FWHM = 151 nm of the optimum aperture function is 53% smaller than the spot corresponding to the full aperture.

The values of depths of printed spots under comparison are smaller than the photoresist thickness on purpose. When this is not the case, there cannot be a valid comparison between the spots, since the overexposure may not lead to a fully recorded spot profile. As was mentioned in section 2, due to the presence of the air/photoresist

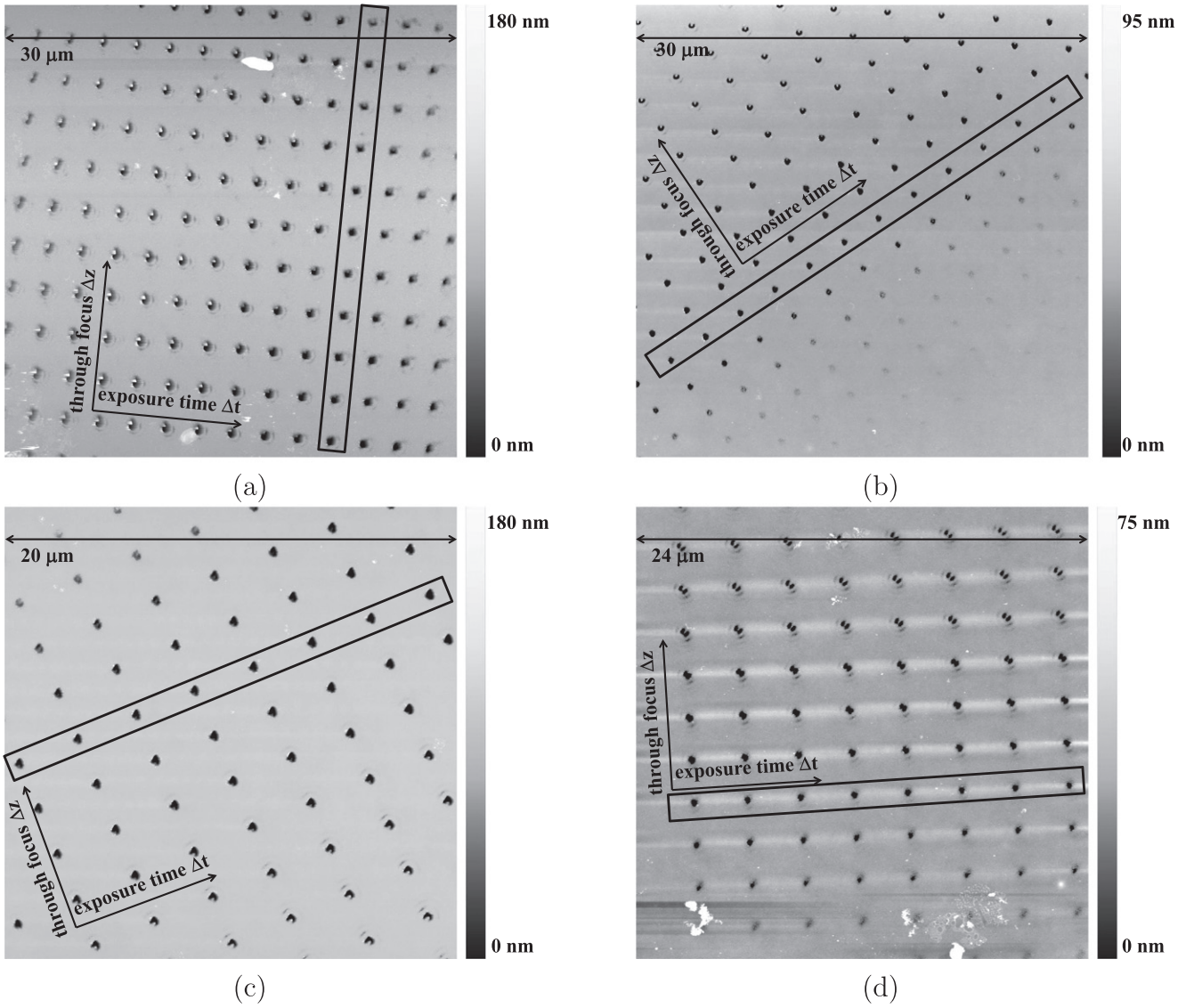

Figure 7. Raw AFM scans of recorded arrays with unmodulated beam intensity profile: (a) reduced aperture modulated intensity amplitude $0.75 < \mathrm{NA} < 0.90$ (b), $0.80 < \mathrm{NA} < 0.90$, (c), optimum amplitude function (d). The marked row corresponds to the best focus and each spot in these rows corresponds to different exposure times.

interface, the longitudinal component is smaller than in the case of focusing in the air. This is also the reason for the choice of the smaller depths of the recorded spots, since in this case the longitudinal component can be isolated using the resist reaction threshold. It should be noted that the size of the recorded spots (both the depth and FWHM) depends on the exposure time. Furthermore, the absolute spot size of the focal spot (FWHM) can be even smaller (it was detected during experiments) if the smaller exposure time is applied. However, relative comparison rather than absolute measurement of the focal spot sizes (FWHM) for different amplitude modulation cases is a goal of the present analysis. Equal depth of the focal spots (for different amplitude modulation cases) is chosen as a criterion for the comparison of the FWHM of the focal spots. Equal depth of the focal spot size is a signature of equal exposure dose delivered to the photoresist and to which the photoresist reacted. For the cases when a range of depths of the best focus spot do not overlap, the contrast parameter = depth/FWHM was calculated and compared as in table 2. Thus, in table 2, the first column gives the depths of the spot. The second, third, fourth, and fifth columns contain FWHM/contrast parameters for the cases of non-modulated, reduced modulated $0.75 < \mathrm{NA} < 0.9$, $0.8 < \mathrm{NA} < 0.9$ apertures, and optimum aperture modulation functions. As discussed in section 2, the simulations shown in figures 2 and 3 indicate that suppression of the transverse component of the field in focus occurs when the center of the beam has zero amplitude. In this way, the total intensity of the field shows a spot with the reduced FWHM, as observed in the experiment. From a comparative analysis of the FWHM parameters obtained experimentally we can see that the case of modulation of the amplitude indeed results in

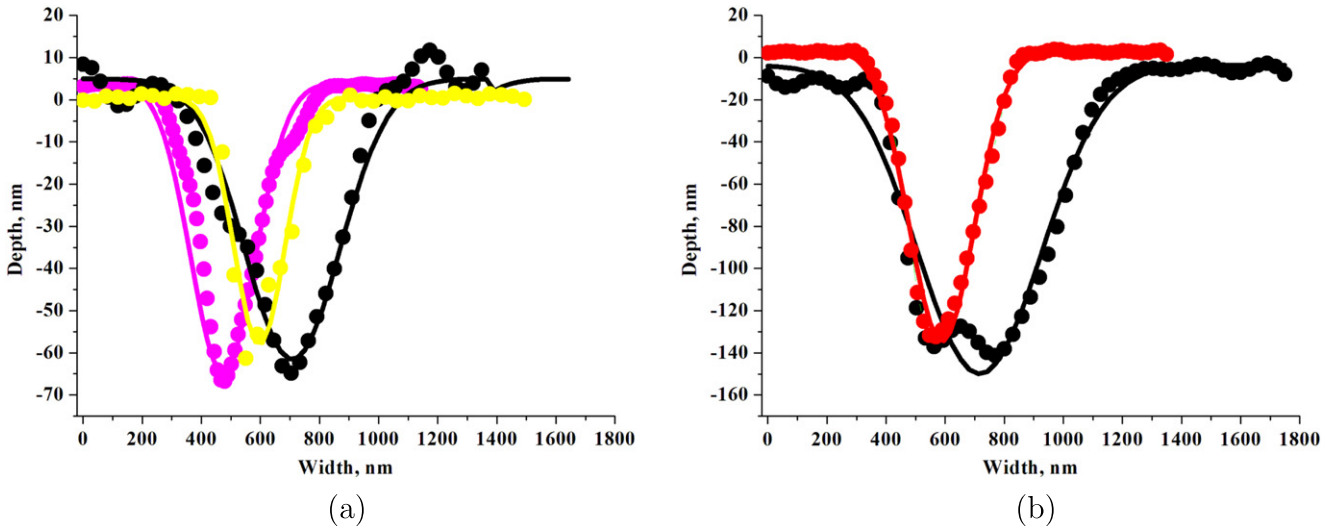

Figure 8. Profiles of raw experimental AFM data for the cases of full $0 < NA < 0.9$ (black), reduced $0.75 < NA < 0.9$ (yellow), and optimum function (magenta) apertures: (a). full $0 < NA < 0.9$ (black) and reduced $0.8 < NA < 0.9$ (red) apertures (b) are illustrated with markers (Fast Fourier fit) and approximated with Gaussian fit solid curves.

Table 2. FWHM, nm/contrast.

Depth, nm	$0 < NA < 0.9$	$0.75 < NA < 0.9$	$0.8 < NA < 0.9$	Optimized function
67	—	173/0.38	—	—
71	323/0.25	—	—	151/0.45
140	419/0.35	—	223/0.67	—

reduction of the spot size, as compared to the case of unmodulated amplitude. Discrepancy in the values of FWHM for experiment and simulations is explainable because the resist has a nonlinear response with the incident light power distribution.

5. Conclusions

Demonstration of the spot-size reduction by means of focusing radially polarized and amplitude modulated light of the wavelength of $\lambda = 405$ nm was shown experimentally and confirmed theoretically. The crucial optical elements of the set-up are spatial light modulator (SLM) to shape required amplitude distributions of two cases of reduced apertures ($0.75 < NA < 0.9$, $0.8 < NA < 0.9$), optimum aperture function implementation and radial polarization of high-quality, shaped by a specially designed wire grid polarizer. After development of the samples, further inspection with optical microscope selects samples for the AFM (atomic force microscope) measurement. Analysis of the FWHM, contrast parameters, extracted from the experimental data was compared for different amplitude modulation cases. The FWHM of the best focused spots, corresponding to the reduced aperture of $0.8 < NA < 0.9$, and optimum aperture function amplitude modulation were 47% and 53% smaller than the one of the full aperture $0 < NA < 0.9$. Simulations based on the Richards–Wolf integral were also performed to confirm experimental results.

Acknowledgments

The authors would like to acknowledge the support of the Stichting voor Technische Wetenschappen (STW project 10727).

References

[1] Khonina S N 2013 *Opt. Eng., Bellingham* **52** 091711
[2] Cuifang Kuang X H X L T W Y K 2011 *Opt. Commun.* **284** 1766–69
[3] Lin H, Jia B and Gu M 2011 *Opt. Lett.* **36** 2471–3
[4] Hu K, Chen Z and Pu J 2012 *Opt. Lett.* **37** 3303–5
[5] Quabis S, Dorn R, Eberler M, Glöckl O and Leuchs G 2000 *Opt. Commun.* **179** 1–7
[6] Zhan Q 2004 *Opt. Express* **12** 3377–82
[7] Dholakia K and Čižmr T 2011 *Nat. Phot.* **5** 335–42
[8] Chen W and Zhan Q 2009 *Opt. Lett.* **34** 722–4
[9] Meier M, Romano V and Feurer T 2007 *App. Phys.* A **86** 329–34
[10] Chen F and de Aldana J R V 2014 *Laser Photon. Rev.* **8** 251–75
[11] Varin C *et al* 2013 *J. Appl. Sci.* **3** 70–93
[12] Ishitobi H, Nakamura I, Hayazawa N, Sekkat Z and Kawata S 2010 *J. Physical Chemistry* B **114** 2565–71

[13] Török P, Varga P and Booker G R 1995 *J. Opt. Soc. Am.* A **12** 2136–44
[14] Dorn R, Quabis S and Leuchs G 2003 *Phys. Rev. Lett.* **91** 233901
[15] Wang H, Shi L, Lukyanchuk B, Sheppard C and Chong C T 2008 *Nat. Phot.* **2** 501–5
[16] Sun C C and Liu C K 2003 *Opt. Lett.* **28** 99–101
[17] Sheppard C J R and Choudhury A 2004 *Appl. Opt.* **43** 4322–7
[18] Khonina S N, Karpeev S V, Alferov S V and Soifer V A 2015 *J. Opt.* **17** 065001
[19] Huse N, Schonle A and Hell S W 2001 *J. Biomed. Opt.* **6** 273–6
[20] Segawa S, Kozawa Y and Sato S 2014 *Opt. Lett.* **39** 4529–32
[21] Scott T F, Kowalski B A, Sullivan A C, Bowman C N and McLeod R R 2009 *Science* **324** 913–7
[22] Sekkat Z and Kawata S 2014 *Laser Photon. Rev.* **8** 1–26
[23] Fourkas J T and Petersen J S 2014 *Phys. Chem. Chem. Phys.* **16** 8731–50
[24] Xu Q and Chen J 2012 *Opt. Commun.* **285** 1642–5
[25] Mathieu L, Juan M R and Quidant R 2011 *Nat. Phot.* **5** 349–56
[26] Padgett M and Bowman R 2011 *Nat. Phot.* **5** 343–8
[27] Tidwell S C, Ford D H and Kimura W D 1990 *Appl. Opt.* **29** 2234–9
[28] Bashkansky M, Park D and Fatemi F K 2010 *Opt. Express* **18** 212–7
[29] Han W, Yang Y, Cheng W and Zhan Q 2013 *Opt. Express* **21** 20692–706
[30] Stalder M and Schadt M 1996 *Opt. Lett.* **21** 1948–50
[31] Wang F, Cai Y, Dong Y and Korotkova O 2012 *Appl. Phys. Lett.* **100** 051108
[32] Grosjean T, Courjon D and Spajer M 2002 *Opt. Commun.* **203** 1–5
[33] Chen W, Han W, Abeysinghe D C, Nelson R L and Zhan Q 2011 *J. Opt.* **13** 015003
[34] Lerman G M and Levy U 2008 *Opt. Lett.* **33** 2782–4
[35] Ghadyani Z, Vartiainen I, Harder I, Iff W, Berger A, Lindlein N and Kuittinen M 2011 *Appl. Opt.* **50** 2451–7
[36] Li X, Cao Y and Gu M 2011 *Opt. Lett.* **36** 2510–2
[37] Urbach H P and Pereira S F 2008 *Phys. Rev. Lett.* **100** 123904
[38] Zhan Q 2009 *Adv. Opt. Photonics* **1** 1–57
[39] Lerman G M and Levy U 2008 *Opt. Express* **16** 4567–81
[40] Ye H *et al* 2013 *Laser Phys. Lett.* **10** 065004
[41] Richards B and Wolf E 1959 *Proc. R. Soc. London* A **253** 358–79
[42] van de Nes A, Billy L, Pereira S and Braat J 2004 *Opt. Express* **12** 1281–93
[43] Urbach H P and Pereira S F 2009 *Phys. Rev.* A **79** 013825
[44] Kotlyar V V, Khonina S N, Kovalev A A, Soifer V A, Elfstrom H and Turunen J 2006 *Opt. Lett.* **31** 1597–9